*Progress In Electromagnetics Research M, Vol. 89, 131–139, 2020*

# Singular Points Meshing Direct Method for Computing the Chaff Radar Cross Section

**Chuan Yin*, Pengquan Zhang, and Zhonghai Zhang**

**Abstract**—An applicable and convenient method is critical for calculating the RCS (Radar Cross Sections) of chaff clouds. An improved method based on direct method is proposed in this paper to promote efficiency, which is called SPMDM (Singular Points Meshing Direct Method). The tanh-sinh method is applied in SPMDM to compute the complex singular function in which the integral domain is meshed by singular points. The practicability and accuracy of the SPMDM are confirmed through comparison with direct method. Results indicate that the SPMDM can significantly decrease calculation time and increase computing efficiency, especially in large-scale case or small relative error region.

## 1. INTRODUCTION

Chaff cloud usually comprises thin wires. Targets, such as planes that require protection, will eject numerous thin wires and form a mass that resembles a cloud. Dipole is a classic form of chaff. To efficiently protect the target, dipoles are cut into a certain length which can resonate in the carrier frequency of radar [1].

Chaff was firstly used for shielding radar detection during the Second World War. Nowadays, chaff is still widely used in military applications, which is launched from an air vehicle to produce a RCS that the radar can identify as a target rather than a real one [2]. Chaff cloud can also be used to study atmospheric air flow in civilian applications [3–5]. In addition, chaff is used for wireless communication, which was studied in [6, 7]. The working efficiency of chaff is determined by a number of parameters, such as physical cross section, loss, flying velocity, sharpness of chaff, sharpness of chaff cloud, volume, falling velocity, and RCS. This paper focuses on RCS, whereas the other parameters are studied in other articles [8–12].

Three different methods were used to calculate the bistatic electromagnetic scattering cross section of a single chaff. The first one is the integer equation method, which was first used in [13]; a new mode based on induced electromotive force was developed in the article. This method was then applied to calculate the backscattering cross section in [14], which was highly consistent with the measured data in [13]. The second method was used to calculate the backscattering of infinitely conducting dipoles in [15]. This method was then applied to finite dipole conductivity in [16]. De Bettencourt utilized this method in a bistatic case [17]. The third method was proposed in [18, 19], which was called the direct method; however, it only carried first-order terms into the calculation which was then improved to two-order terms in [20, 21], and it was more complicated than the former one but provided a complete description of the scattering cross section. Stokes parameters were then applied in the direct method to demonstrate the necessity of four independent quantities in determining chaff cross section. The Monte Carlo method was also used to evaluate averages over wire orientations. Unfortunately, Dedrick et al. [22] in relation to polarizations was defined with respect to the scattering plane. Moreover, numerical work that relied on the Monte Carlo method resulted in significant errors, which were identified and

*Received 21 November 2019, Accepted 17 January 2020, Scheduled 1 February 2020*
* Corresponding author: Chuan Yin (yinc@hdu.edu.cn).
The authors are with the HangDian University, Hangzhou 310018, China.

addressed in [1]. Based on the direct method, an improved model was applied in [1], wherein spherically averaged bistatic cross sections were applied to a cloud of randomly positioned and randomly oriented resonant dipoles. This study also identified and addressed the errors in [22] using the new results. The resonance effects of chaff were considered in [23] combined with the work of the former. The influence of chaff on RCS was studied, and the comprehensive three-dimensional graphs of the relevant bistatic cross sections plotted against scattering angle and frequency were presented. However, these methods assume that the contribution phase to the RCS from each fiber is random. This assumption is invalid for the forward scatter direction. A completely different RCS for forward scattering was then realized in [24]. Numerically intensive methods that require long computation times were proposed to compute bistatic RCS for all directions [25]. A unified method was then proposed to determine the total average RCS of a spherical chaff cloud [26]; this method was valid for all scattering directions, including forward scatter. A novel chaff cloud Radar Cross Section (RCS) model was proposed to characterize battle ship auto protection systems under operational configurations [27], in which the software, called SILEM, has been developed to calculate decoy placement, chaff cloud evolution and dispersion, and radar scattering by dipoles.

A complete high efficient solution to the bistatic scattering problem from chaff cloud has not yet been developed. To solve the problem, SPMDM is proposed in this paper that combines the tanh-sinh method [29] with the direct method. This paper is organized as follows. Section 2 presents the detailed problem mentioned above. The tanh-sinh method is compared with the Gauss method [21] in Section 3.1 to verify the high accuracy of the former. Finally, the RCSs of dipole and chaff clouds are calculated with SPMDM in Section 3.2. The results of SPMDM are compared with the direct method to prove the accuracy and high efficiency of the proposed method.

## 2. PROBLEM DEFINITION

The overall geometry applicable to bistatic scattering is shown in Fig. 1. A transmitting antenna located at point T radiates an arbitrarily polarized wave toward a cloud of randomly positioned and oriented dipoles denoted as point D. The transmitting direction is defined by spherical coordinate angles $(\theta_1, \varphi_1)$, defined in the common $X$, $Y$, and $Z$ coordinate frame. The dipole cloud is sufficiently far, and the

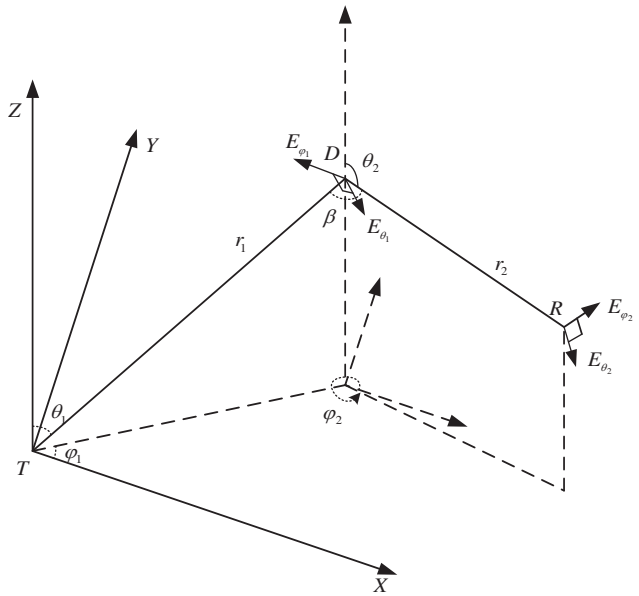


**Figure 1.** Overall coordinates of the bistatic scattering.

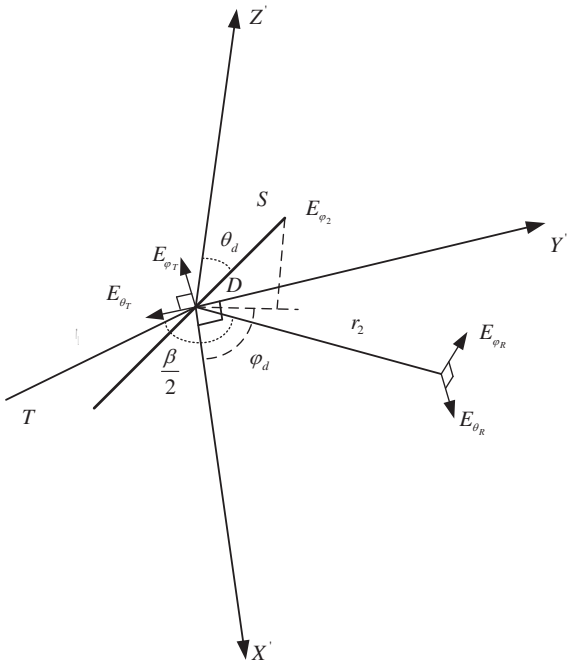


**Figure 2.** Local coordinate of the scattering and dipole.

incident wave can be considered as a planar wave. The chaff is assumed sufficiently smaller than the average distance $r_1$. Thus, the strength of the incident field is approximately the same for all dipoles. Moreover, the dipoles are assumed sufficiently sparse. Thus, the scattering between the dipoles and mutual coupling can be neglected. A receiver located at point R is defined by spherical angles $(\theta_2, \varphi_2)$. The receiving antenna is also assumed far enough away from the cloud. Thus, distance between the chaff and receiver is approximately equal to average distance $r_2$. The angle between $TD$ and $DR$ is denoted by $\beta$. The electric field of the incident wave $E_1$ can be resolved into two polarized directions, namely, $E_{\theta_1}$ and $E_{\varphi_1}$. The electric field vector is denoted by $E_2$. The wave arriving at the receiver similarly comprises two directions, namely, $E_{\theta_2}$ and $E_{\varphi_2}$.

The relationship between the electric field of incident wave and received wave cannot be indicated by the overall coordinate as the orientation of the dipoles is randomly distributed. The local coordinate is set up in Fig. 2 to solve this problem. Plane TDR is the scattering plane. Local coordinate system $X'$, $Y'$, $Z'$ are defined as the $X'$ and $Y'$ axes that lie on the plane TDR. The $X'$ axis bisects scattering angle $\beta$. $E_{\varphi_T}$ lies on the scattering plane, which is defined as the incident electric field components. Another incident electric field component is defined by $E_{\theta_T}$. Received electric fields $E_{\theta_R}$ and $E_{\varphi_R}$ are also defined in the figure.

The dipole is denoted by $S$, whose direction is $(\theta_d, \varphi_d)$. By using the polarization scattering matrix approach to the scattering problem, the relationship between $E_{\varphi_R}$, $E_{\theta_R}$ and $E_{\theta_T}$, $E_{\varphi_T}$ can be presented by [1]

$$\begin{bmatrix} E_{\theta_R} \\ E_{\varphi_R} \end{bmatrix} = \begin{bmatrix} d_{11} & d_{12} \\ d_{21} & d_{22} \end{bmatrix} \begin{bmatrix} E_{\theta_T} \\ E_{\varphi_T} \end{bmatrix}. \tag{1}$$

Field components $E_{\theta_T}$ and $E_{\varphi_T}$ are related to the transmitted field $E_{\theta_1}$ and $E_{\varphi_1}$, respectively, which are incidents on the dipole:

$$\begin{bmatrix} E_{\theta_T} \\ E_{\varphi_T} \end{bmatrix} = \begin{bmatrix} T_{11} & T_{12} \\ T_{21} & T_{22} \end{bmatrix} \begin{bmatrix} E_{\theta_1} \\ E_{\varphi_1} \end{bmatrix}. \tag{2}$$

Field components $E_{\varphi_R}$ and $E_{\theta_R}$ are related to $E_{\theta_2}$, $E_{\varphi_2}$, which can be expressed by

$$\begin{bmatrix} E_{\theta_2} \\ E_{\varphi_2} \end{bmatrix} = \begin{bmatrix} R_{11} & R_{12} \\ R_{21} & R_{22} \end{bmatrix} \begin{bmatrix} E_{\theta_R} \\ E_{\varphi_R} \end{bmatrix}. \tag{3}$$

Thus, the following equation is obtained by combining Eqs. (1) and (2) with Eq. (3):

$$\begin{bmatrix} E_{\theta_2} \\ E_{\varphi_2} \end{bmatrix} = [R]\,[D]\,[T] \cdot \begin{bmatrix} E_{\theta_1} \\ E_{\varphi_1} \end{bmatrix}, \tag{4}$$

where matricrs $[R]$ and $[T]$ can be easily obtained in [1]. The critical problem is to solve matrix $[D]$, which represents scattering matrix of the dipole. In the local coordinate, current $I_T$ is in the center of a dipole with a sinusoidal current distribution, and the effective lengths are in the interest direction of $(\theta, \varphi)$. Thus,

$$[h_\theta, h_\varphi] = A(\theta, \varphi)[-\sin\theta\cos\theta_d + \cos\theta\sin\theta_d\cos(\varphi - \varphi_d), \sin\theta_d\sin(\varphi_d - \varphi)] \tag{5}$$

where $A(\theta, \varphi)$ is denoted as

$$A(\theta, \varphi) = \frac{(\lambda/\pi)}{\sin(\pi L/\lambda)} \frac{\cos[(\pi L/\lambda)\cos\psi] - \cos(\pi L/\lambda)}{\sin^2\psi}, \tag{6}$$

where $\cos\psi$ is

$$\cos\psi = \cos\theta\cos\theta_d + \sin\theta\sin\theta_d\cos(\varphi - \varphi_d). \tag{7}$$

As shown in Fig. 2, plugging point R located in the scattering direction with the spherical coordinates $(r_2, \pi/2, \beta/2)$ into Eqs. (5)–(7) [28] allows the dipole to radiate toward point R; thus, the following equation is obtained [19]

$$\begin{bmatrix} E_{\theta_R} \\ E_{\varphi_R} \end{bmatrix} = \frac{-\mathrm{j}\eta I_T}{2\lambda r_2} \exp(-\mathrm{j}2\pi r_2/\lambda) \begin{bmatrix} h_\theta(\pi/2, \beta/2) \\ h_\varphi(\pi/2, \beta/2) \end{bmatrix}, \tag{8}$$

where $\eta = 120\pi$ is the intrinsic impedance of the free space, and $I_T$ is generated from the radiate of incident wave

$$I_T = V_{0c}/Z_{rad} = [E_{\theta_T} h_\theta(\pi/2, -\beta/2), -E_{\varphi_T} h_\varphi(\pi/2, -\beta/2)]/Z_{rad}. \tag{9}$$

In Eq. (9), $Z_{rad}$ is the impedance of the dipole. By combining Eqs. (2), (8), and (9) [1], matrix $[D]$ can be obtained by

$$[D] = \begin{bmatrix} d_{11} & d_{12} \\ d_{21} & d_{22} \end{bmatrix}, \tag{10}$$

where

$$d_{11} = BA_0(\beta/2)\cos^2\theta_d, \tag{11a}$$

$$d_{12} = BA_0(\beta/2)\cos\theta_d \sin\theta_d \sin(\varphi_d + \beta/2), \tag{11b}$$

$$d_{21} = -BA_0(\beta/2)\cos\theta_d \sin\theta_d \sin(\varphi_d - \beta/2), \tag{11c}$$

$$d_{22} = -BA_0(\beta/2)\sin^2\theta_d \sin(\varphi_d - \beta/2), \tag{11d}$$

where

$$B = [-\mathrm{j}\eta/(2\lambda z_{rad} r_2)]\exp(-\mathrm{j}2\pi r_2/\lambda), \tag{12}$$

$$A_0(\beta/2) = A(\pi/2, \beta/2)A(\pi/2, -\beta/2). \tag{13}$$

The RCS of the dipole is then given by Eqs. (14a)–(14c), in which $\sigma_{ptop}(p \in (\perp, //))$ is the Radar Cross Section of the dipole, assuming that angles $\theta_d$ and $\varphi_d$ are uniformly distributed in $(0, \pi)$ and $(0, 2\pi)$.

$$\sigma_{\perp to \perp} = 4\pi r_2^2 |B|^2 \int_0^{2\pi}\int_0^{\pi} A_0^2(\theta_d, \varphi_d)\cos^4\theta_d \sin\theta_d d\theta_d d\varphi_d, \tag{14a}$$

$$\sigma_{\perp to //} = 4\pi r_2^2 |B|^2 \int_0^{2\pi}\int_0^{\pi} A_0^2(\theta_d, \varphi_d)\cos^2\theta_d \sin^3\theta_d \sin^2(\varphi_d + \beta/2) d\theta_d d\varphi_d, \tag{14b}$$

$$\sigma_{//to//} = 4\pi r_2^2 |B|^2 \int_0^{2\pi}\int_0^{\pi} A_0^2(\theta_d, \varphi_d)\sin^5\theta_d \sin^2(\varphi_d - \beta/2)\sin^2(\varphi_d + \beta/2) d\theta_d d\varphi_d, \tag{14c}$$

where

$$A_0^2(\theta_d, \varphi_d) = \frac{(\lambda/\pi)^2}{\sin(\pi L/\lambda)^2}\left(\frac{\cos[(\pi L/\lambda)\sin\theta_d \cos(\beta/2 - \varphi_d)] - \cos(\pi L/\lambda)}{1 - \sin^2\theta_d \cos^2(\beta/2 - \varphi_d)}\right)^2 \left(\frac{\cos[(\pi L/\lambda)\sin\theta_d \cos(-\beta/2 - \varphi_d)] - \cos(\pi L/\lambda)}{1 - \sin^2\theta_d \cos^2(-\beta/2 - \varphi_d)}\right)^2 \tag{15}$$

The RCS of the dipole can then be obtained by combining Eqs. (14a)–(14c) and (15) [24]. The computation and discussion are presented in the following section.

## 3. EXPERIMENTS AND ANALYSIS

The chaff cloud is assumed to be randomly distributed. Spherical average is implemented during calculation to deal with chaff orientation. The accuracy and efficiency of the integration algorithm directly determine the accuracy of the RCS. Thus, a practical and highly efficiency integration algorithm is significant in calculating the RCS of the chaff.

The Monte Carlo method is widely used to solve this problem. However, the tremendous computation requirements limit its application in complex scene. Therefore, SPMDM that combines the tanh-sinh algorithm with the direct method is proposed in this paper to solve this problem.

### 3.1. Comparison with Gauss Integration Method

In this section, the high accuracy of the tanh-sinh algorithm in a singular function is verified by comparing Gauss integration method with the tanh-sinh method.

As a typical numerical integration method, Gauss integration is widely applied in non-singular function. However, this method has a poor performance when the non-singular function is replaced by a singular one. The relative errors of Gauss integration with the number of interpolation points are shown in Fig. 3. In this figure, the singular function is $1/\sqrt{x^2+y^2}$, and the range of the integration is $x \in (0,1)$, $y \in (0,1)$; $x \in (0,0.5)$, $y \in (0,0.5)$; and $x \in (0,2)$, $y \in (0,2)$. The tanh-sinh algorithm is used to increase the accuracy of the results in this paper.

Tanh-sinh, which was mainly used to solve the one-dimensional problem in the early stage, was first proposed in 1973 [29]. However, tanh-sinh is rarely discussed, and a few details are provided in [30, 31]. The key feature of tanh-sinh method is locating the interpolate point. The interpolate points are nearly uniformly distributed on the integration range for Gauss integration method. To verify the reliability of the case in which tanh-sinh is applied on the singular function with the singular point right on the boundary, the singular function $1/\sqrt{x^2+y^2}$ is also integrated on the range of $x \in (0,1)$, $y \in (0,1)$ with the tanh-sinh method. The results are shown in Fig. 4.

The relative errors of tanh-sinh method are significantly lower than those of the Gauss method. The decline rate of the tanh-sinh method is also significantly faster than that of the latter method. The results in Figs. 3 and 4 indicate that the tanh-sinh algorithm is an appropriate method for singular function. The tanh-sinh algorithm is then combined with the direct method to calculate the RCS of the dipole.

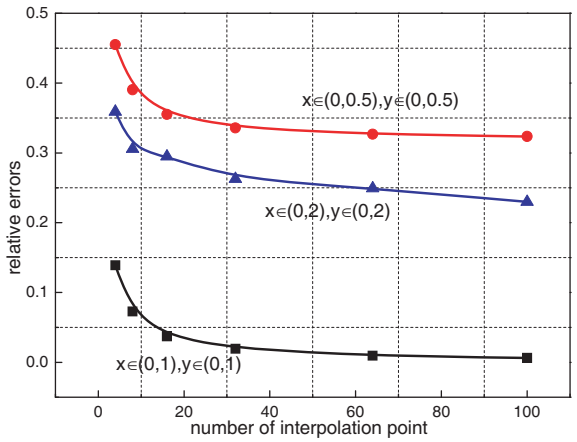


**Figure 3.** Relative errors with the number of interpolation points in the Gauss integration method.

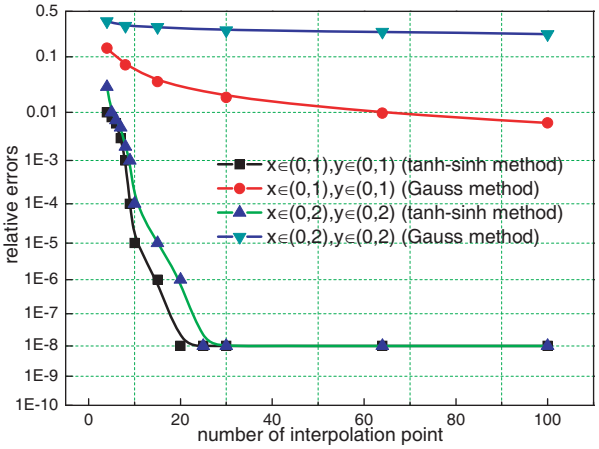


**Figure 4.** Relative errors with the number of interpolate points in tanh-sinh method.

### 3.2. Computing the RCS of the Dipole

The tanh-sinh method is used to compute the RCS of the dipole, and the spherically averaged bistatic radar cross sections for linearly polarized transmission and reception are shown in Fig. 5 and Fig. 6.

The results indicate that the curves obtained by the tanh-sinh method are significantly different from the Monte Carlo method. The reason is that in Equations (13)–(15), the four singularities of the integrand are away from the boundary of the integration area; however, the singularity should be near the boundary of the integration area when using tanh-sinh method.

To solve the problem, SPMDM is proposed in which the integration area is divided into fourteen parts, and the four points are right on the vertex of each part, which is shown in Fig. 7. Then, the RCS of the dipole is the sum of the fourteen parts.

Two different parameters of the dipole are calculated with SPMDM, and the results are shown in Figs. 8 and 9. The results indicate that the curves obtained by the SPMDM are consistent with

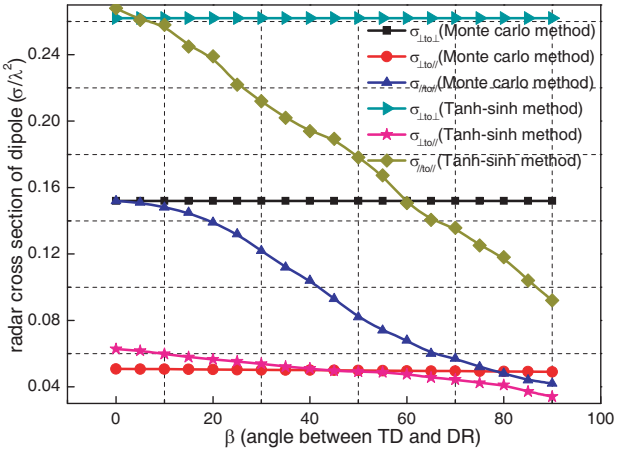


**Figure 5.** Comparison of the tanh-sinh method with the Monte carlo method. The impedance and the length of the dipole are $Z_{rad} = 73.0\,\Omega$, $L = \lambda/2$.

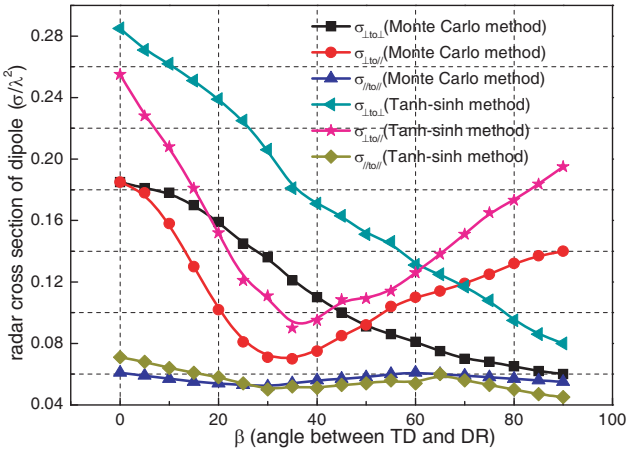


**Figure 6.** Comparison of the tanh-sinh method with the Monte carlo method. The impedance and the length of the dipole are $Z_{rad} = 105.4\,\Omega$, $L = 3\lambda/2$.

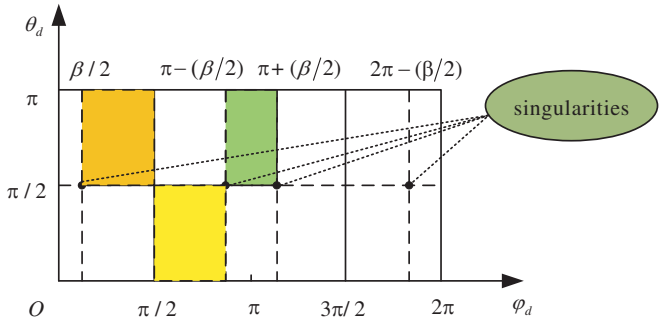


**Figure 7.** Meshed integration area of the RCS.

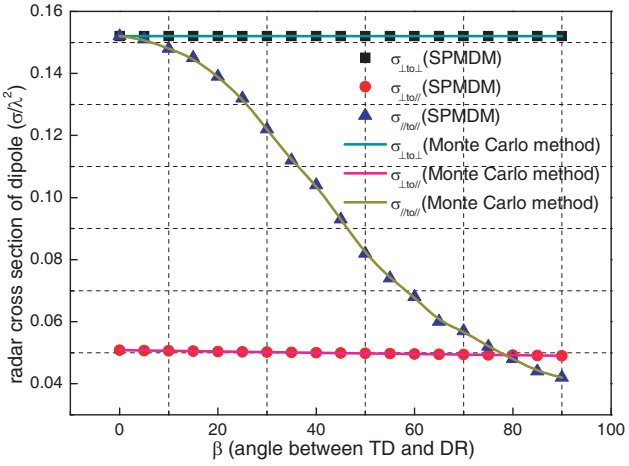


**Figure 8.** Spherically averaged bistatic radar cross sections for linearly polarized transmission and reception. The impedance and the length of the dipole are $Z_{rad} = 73.0\,\Omega$, $L = \lambda/2$.

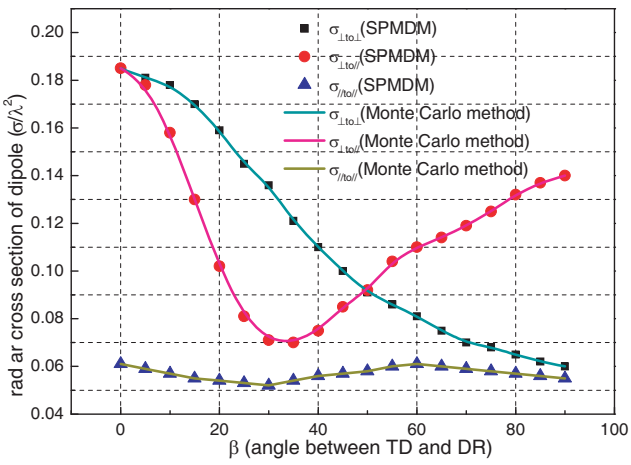


**Figure 9.** Spherically averaged bistatic radar cross sections for linearly polarized transmission and reception. The impedance and the length of the dipole are $Z_{rad} = 105.4\,\Omega$, $L = 3\lambda/2$.

the direct method in which the Monte Carlo method was used to calculate the singular function [1]. Furthermore, it is also seen that the SPMDM can significantly increase the accuracy of the results compared with the original tanh-sinh method.

In addition, the SPMDM is applicable for computing the averaged RCS of the chaff cloud. The computing time of SPMDM is then compared with the direct method to verify the high efficiency of the proposed method.

The relative errors of the RCS with the computing time are presented in Figs. 10 and 11. Three different numbers of chaffs are also calculated as 20, 2000, and 200000. The results indicate that the relative errors of both methods decrease with the increase of computing time, and the computing time also increases with the number of chaffs increases. Moreover, the results also show that the SPMDM takes significantly less time than the direct method for the same scale case

In order to indicate the relationship of the two method more clearly. The comparison of the two method is presented in Fig. 12 and Fig. 13.

The computing time of the two methods with the relative errors are shown in Fig. 12. It is seen that the computing times of both methods increase with the decrease of relative errors. In the range of error above 1e-6, the blue line exhibits a slope nearly linear, a characteristic drastically different from the green one, which takes a quadratic shape. Thus, the high efficiency of the SPMDM in small relative

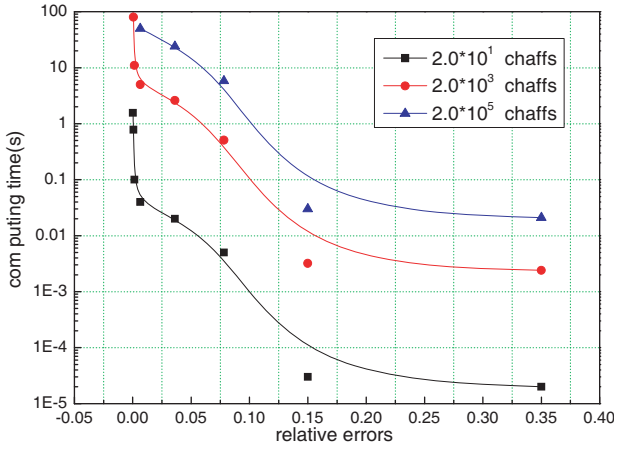


**Figure 10.** Computing time with the relative errors of RCS by the direct method.

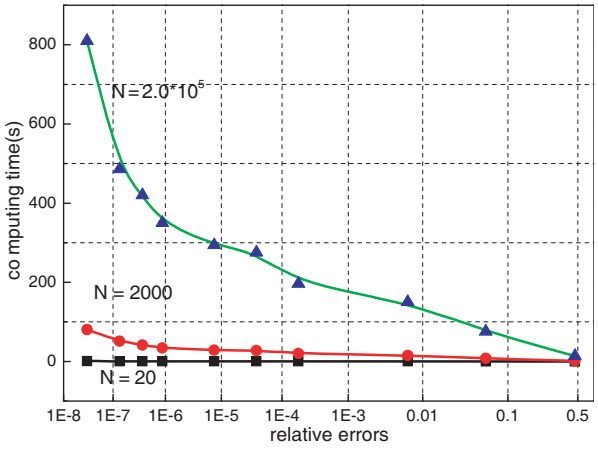


**Figure 11.** Computing time with the relative errors of RCS by the SPMDM.

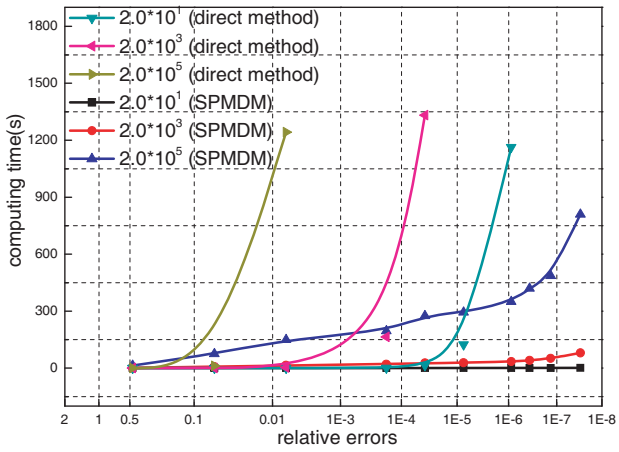


**Figure 12.** Computing time of the two method with the relative errors.

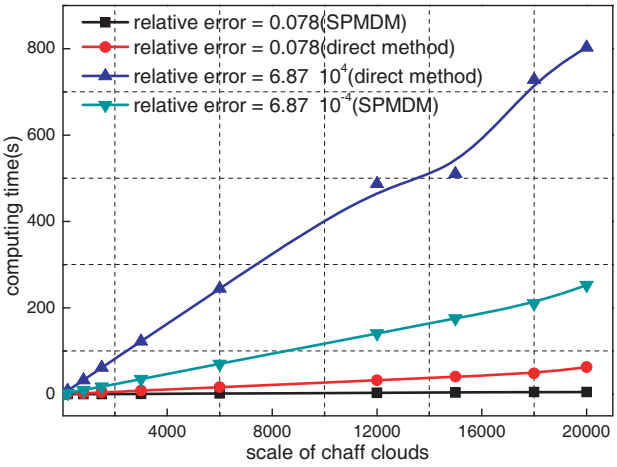


**Figure 13.** Computing time of the two methods with the scale of chaff clouds.

error region is verified by comparison with the direct method.

The computing times of the two methods with the number of chaffs are shown in Fig. 13. It is seen that the computing time of both methods almost linearly increase with increasing number of chaffs, and the computing time of SPMDM is significantly shorter than that of the direct method, especially in large-scale case. Then, with the increase of the scale, the slope of the SPMDM is also much smaller than that of the direct method in the same relative errors.

## 4. CONCLUSIONS

An improved method called SPMDM is proposed in this paper, in which the tanh-sinh method is used to compute the complex singular function. The proposed method is applied to calculate the RCS of the chaff clouds.

During the calculation of SPMDM, the integration area is divided into fourteen parts to improve the accuracy of RCS of the chaff clouds. It is found that the curves obtained by the SPMDM are consistent with the direct method in which the Monte Carlo method is used to calculate the singular function. Moreover, the relative errors of the RCS with the computing time are studied in this paper. Results indicate that the relative errors of both methods decrease with computing time. Computing time also increases with the number of chaffs. Moreover, the computing time of the SPMDM is much less than the original method in the same scale case. Then, relative errors of the RCS with the computing time of different methods are studied by comparing different scales of chaff cloud. Results reveal that the computing time of both methods almost linearly increase with the chaff number, and the computing time of the SPMDM is significantly shorter than that of the direct method. With the increase of the scale, the slope of the SPMDM is also much smaller than that of the direct method in the same relative errors. Furthermore, the high efficiency of the SPMDM in small relative error region is verified by comparison with the direct method. The SPMDM can significantly decrease the calculation time and increase the computing efficiency.

## ACKNOWLEDGMENT

This work is supported by the National Natural Science Foundation of China under grant numbers 61801153, State Key Laboratory of Millimeter Waves under grant numbers K202012 and Natural Science Foundation of ZheJiang province (LQY20F010001).

## REFERENCES

1. Peyton, Z. and J. R. Peebles, "Bistatic radar cross sections of chaff," *IEEE Transaction on Aerospace and Electronic Systems*, Vol. 20, No. 2, 128–140, 1984.
2. Sun, P., Q. Cai, J. Tang, et al., "On spreading chaff cloud for countering the terminal guidance missile," *IEEE Cie International Conference on Radar. IEEE*, 845–849, 2012.
3. Ceperuelo, M., M. C. Llasat, L. López, et al., "Study of 11 September 2004 hailstorm event using radar identification of 2-D systems and 3-D cells," *Advances in Geosciences*, 7, 2006.
4. Martner, B. E., J. D. Marwitz, and R. A. Kropfli, "Radar observations of transport and diffusion in clouds and precipitation using TRACIR," *Journal of Atmospheric & Oceanic Technology*, Vol. 9, No. 3, 226–241, 1992.
5. Klimowski, B. A., R. Becker, E. A. Betterton, et al., "The 1995 Arizona program: Toward a better understanding of winter storm precipitation development in mountainous terrain," *Bulletin of the American Meteorological Society*, Vol. 79, No. 5, 799–813, 1998.
6. Tang, B., K. Y. Guo, J. P. Wang, et al., "The correlation characteristics of channel matrix of chaff-supported MIMO system," *IEEE Ant. & Wireless Propagat. Letts.*, Vol. 13, 1509–1512, 2014.
7. Tang, B., H. M. Li, and X. Q. Sheng, "Jamming recognition method based on the full polarisation scattering matrix of chaff clouds," *IET Microwaves Antennas & Propagation*, Vol. 6, No. 13, 1451–1460, 2012.

8. Hang, H., Z. Tong, S. Chai, and Y. Zhang, "Experimental and numerical study of chaff cloud kinetic performance under impact of high speed airflow," *Chinese Journal of Aeronautics*, Vol. 31, No. 11, 2080–2092, 2018.
9. Li, Z. H. and L. S. Wang, "Modeling study on holistic kinetic performance of chaff cloud," *Journal of System Simulation*, Vol. 21, No. 4, 928–877, 2009.
10. Li, Z. H., J. Liang, S. X. Li, et al., "Computing study on holistic aerodynamics of chaff cloud covering various flow regimes," *Acta Aerodynamica Sinica*, Vol. 29, No. 1, 59–67, 2011.
11. Lv, M. M., "Motion characteristics of chaff cloud in the air," *Electronic Component & Device Applications*, 2012.
12. Feng, D. J., X. S. Wang, and J. Q. Liu, "Jamming effect analysis of chaff cloud on ground-based radar and its application," *Modern Radar*, 2010.
13. VanVleck, J. H., F. BIoch, and M. Hammermesh, "Theory of radar reflections from wires and thin metallic strips," *Journal of Applied Physics*, Vol. 18, No. 3, 274–294, 1947.
14. Dike, S. H. and D. D. King, "The absorption gain and backscattering cross section of the cylindrical antenna," *Proceeding of IRE*, Vol. 40, No. 7, 853–860, 1952.
15. Tai, C. T., "Electromagnetic backscattering from cylindrical wires," *Journal of Applied Physics*, Vol. 23, 909–916, 1952.
16. Cassedy, E. S. and J. Fainberg, "Back scattering cross sections of cylindrical wires of finite conductivity," *IRE Transactions on Antennas and Propagation*, Vol. 8, No. 1, 1–70, 1960.
17. De Bettencourt, J. T., "Bistatic cross sections of cylindrical wires," *Sci. Rep. Inc.*, Needham, MA, 1961.
18. Ufimtsev, P. Ya., "Diffraction of plane electromagnetic waves by a thin cylindrical conductor," *Radio Eng. Electron. Phys.*, Vol. 7, No. 3, 241–249, 1962.
19. Fialkovskii, A. T., "Scattering of plane electromagnetic waves by a thin cylindrical conductor of finite length," *Soviet Phys. Tech. Phys.*, Vol. 11, No. 1, 1300–1304, 1967.
20. Einarsson, "The current distribution on cylindrical antennas of arbitrary length," *Trans. Roy, Inst. Tech. Stockholm*, 1963.
21. Hallen, E., *Electromagnetic Theory*, Wiley, New York, 1962.
22. Dedrick, K. G., A. R. Hessing, and G. L. Johnson, "Bistatic radar scattering by randomly oriented wires," *IEEE Transactions on Antennas and Propagation*, Vol. 26, No. 3, 420–426, 1981.
23. Ashrafi, D., H. Uberall, and A. Nagl, "The resonance structure of the bistatic radar scattering cross section of randomly oriented dipoles," *Journal of Electromagnetic Waves and Applications*, Vol. 6, No. 7, 975–994, 1992.
24. Guo, Y. and H. Uberall, "Bistatic radar scattering by a chaff cloud," *IEEE Transactions on Antennas and Propagation*, Vol. 40, No. 7, 837–841, 1992.
25. Cross, J. L., "Response of arrays to stochastic fields," Ph. D. Dissertatio, University of Florida, Gainesville, 1969.
26. Marcus, S. W., "Bistatic RCS of spherical chaff clouds," *IEEE Transactions on Antennas and Propagation*, Vol. 63, No. 9, 4091–4099, 2015.
27. Pinchot, J. L., O. Béchu, and P. Pouliguen, "A chaff cloud modelisation," *IEEE International Symposium on Antenna Technology & Applied Electromagnetics*, 2017.
28. Butter, B. C. and F. Chaff, "Communications, radar and signal processing," *IEEE Proceedings*, Vol. 129, No. 3, 197–201, 1982.
29. Takahasi, H. and M. Mori, "Double exponential formulas for numerical integration," *European Mathematical Society Publishing House*, Vol. 9, No. 3, 721–741, 1973.
30. Baileya, D. H., K. Jeyabalanb, and X. S. Li, "A comparison of three high-precision quadrature schemes," *Experimental Mathematics*, Vol. 14, No. 3, 317–329, 2005.
31. Baileya, D. H., Borwein, and M. Jonathan, "Highly parallel, high-precision numerical integration," Lawrence Berkeley National Laboratory, 2005.